Calculation of effective elastic moduli of polycrystalline materials including nontextured samples and fiber textures

H. Kiewel and L. Fritsche
Institut für Theoretische Physik der Technische Universität Clausthal, Leibnizstrasse 10, D-38678 Clausthal-Zellerfeld, Germany
(Received 22 February 1994)

We report an improved version of a recently developed method that allows the calculation of effective elastic constants of polycrystalline materials. The method is predicated on the idea that the system can be described by a homogeneous substitute material which obeys Hooke's law with elastic constants that define the macroscopic elastic properties of the original system. In order to determine these constants, one cuts out of a parallelepiped section and replaces it with a cluster of 100–500 grains of the original material. For simplicity we have provisionally assumed these grains to have a shape of rectangular columns. The cluster is connected to the embedding system by invoking the usual boundary conditions. The entire system is subject then to a set of linear independent homogeneous deformations whose number has to be chosen large enough to determine the sought-for independent elastic constants of the substitute system. The method yields apart from these constants also the entire displacement field within the cluster, and hence provides interesting additional information.

I. INTRODUCTION

In many situations where elastic properties of polycrystalline materials play a role they are assessed by the response to stresses that probe a macroscopic section of the material containing a large number of grains. To reliably calculate the effective elastic constants which give an appropriate description of those materials appear to be very desirable from a practical point of view. In the case of isotropic polycrystalline materials whose elastic properties are described by two elastic constants one can argue that the latter result from averaging the individual compliances of the grains over all grain orientations as it occurs when the system is exposed to a constant stress throughout the sample. The moduli thus defined have been introduced by Reuss.[1] Voigt[2] had earlier advanced an alternative definition that consisted in forming the average of the individual grain stiffnesses over the orientation space which amounts to having a constant strain everywhere in the sample. As has been shown by Hill,[3] the values obtained by Reuss and Voigt constitute, respectively, the lower and upper bounds of the pertinent effective moduli of the material. To extend the original idea of Reuss and Voigt to textured materials, one can form a weighted average over the orientation space by incorporating an experimentally determined orientation distribution function (ODF).

The definitions of the Reuss-Voigt values imply that the effect of the grain interaction is negligible. To go beyond that level of approximation Hershey[4] forwarded a method that allowed one to deal with this interaction in a simplified form. The model underlying his method consists of embedding a representative spherical grain in an elastically isotropic matrix that simulates the macroscopic properties of the polycrystalline material. This approach was further pursued by Eshelby[5] and developed into an exact method by Kröner[6] for perfectly uncorrelated polycrystals. The original Hershey-Kröner idea of exactly treating a spherical grain embedded in a macroscopic substitute system has been worked out in detail and been applied to a large variety of polycrystals by Kneer.[7,8] His results stand out by an impressive accuracy in describing the experimental moduli. He could in addition demonstrate that one can successfully treat textured materials within this framework as well.

The initial limitation to completely uncorrelated polycrystals was later removed by Kröner and Green's-function approach to the problem in question. The new method is based on transforming the basic differential equation for the elastic displacement into an integral equation that bears a strong resemblance to the Lippmann-Schwinger equation familiar from the scattering problem in quantum mechanics. One can benefit to some extent from this correspondence which has been exploited to the fullest by Kröner[9] and forcefully been advanced by Zeller and Dederichs.[10] Primarily, the displacement field appears now expressed as an integral which contains the Green's function of a homogeneous medium and, as a central information on the grain structure and their elastic properties the real-space-dependent deviation of the elastic constants from some suitably chosen constant values which the Green's function refers to. In recasting this interconnection and introducing n-point correlation functions for the distribution of the (now space-dependent) elastic constants Kröner arrives at an exact relation between the sought-for effective moduli and those correlation functions. Within this framework it is possible to define lower and upper bounds for these moduli with reference to certain classes of correlation. The bounds derived by Hashin and Shtrikman[11,12] prove to fall into this classification. As they are primarily obtained by these authors from a variational principle for the elastic deformation energy of the polycrystalline material, the bounds lie closer together than those by Reuss

0163-1829/94/50(1)/5(12)/$06.00

and Voigt. The "Lippmann-Schwinger" version of a possible access to the problem in question is mathematically rather involved, and its feasibility depends on the convergence of Born-type series in terms of which the solution of the Lippmann-Schwinger equation can be expressed. Porous materials pose a serious problem in that context. But there is a number of other practical obstacles that have so far impeded a development of the method into a viable tool.

The philosophy of tackling a mathematical problem in various disciplines of theoretical physics has in the past decade been strongly influenced by the vastly improved capacity of modern electronic computers. This is vividly reflected in the spread of Monte Carlo methods that have been used, for example, to directly solve the many-particle Schrödinger equation, or the modern approach to molecular dynamics where one simulates the properties of thermodynamical systems by directly integrating Newton's equations. The theoretical concept of the present paper is much in the line of this development in that we are aiming at a straightforward integration of the fundamental differential equation for the displacement field of a realistic polycrystal. An outline of our approach has already been given in an earlier paper.[13] The work of Kumar[14] is similar in its point of view but pursues a mathematically quite different line of thought by employing the method of finite elements.

Our approach consists in solving the fundamental equation for the elastic displacement in a sufficiently large cluster of grains subject to a homogeneous deformation everywhere at the surface of the cluster. One is then in the position to determine the strains and stresses everywhere in the cluster and to form the volume averages of them. The fourth-rank tensor interconnecting these averages constitutes the sought-for effective stiffnesses of the macroscopic sample. In practice, we reduce the solution of the pertinent differential equation with the inclusion of the familiar boundary conditions at the grain surfaces partly to an algebraic problem. We expand the displacement inside the grains in terms of basis functions which satisfy the differential equation individually. Since these—in principle, infinite—expansions have to be truncated, a finite error in the boundary conditions occurs which can be used to determine the expansion coefficients by requiring that the mean-square error attains a minimum. The latter condition leads to a set of linear inhomogeneous equations.

The plan of the paper is as follows. In Sec. II, we give a detailed description of our approach. We apply our scheme to a large variety of macroscopically isotropic materials ranging from polycrystalline cubic metals to graphite and superconducting ceramics. Where reliable experimental values are available for a comparison, our result show very satisfactory agreement. A particular virtue of our method can be seen in its flexibility to handle near spherical grains as well as plate and needle-shaped crystallites. The latter occur in strongly textured materials. We give an example of the functioning of our method for a copper fiber texture displaying the familiar ideal orientations for fcc metals. To demonstrate the capability of our method to provide additional information, e.g., on the details of the displacement field, we show some plots on the deformation in heterogeneous systems. The material of these results is compiled in Sec. III.

II. THEORY

Since we are only interested in the calculation of effective elastic moduli we may confine ourselves to purely static deformations. In addition we neglect any kind of external forces acting on the unit volume. The fundamental equations governing the behavior of elastic media in a state of static equilibrium are then given by

$$\nabla\cdot\underline{\sigma}(\mathbf{r})=0 \tag{2.1}$$

and by Hooke's law

$$\sigma_{ij}(\mathbf{r})=\sum_{k,l}c_{ijkl}\epsilon_{kl}(\mathbf{r}) \tag{2.2}$$

provided that the strains described by the tensor $\underline{\epsilon}$ are small compared to unity. The stress tensor is denoted by $\underline{\sigma}$, and the quantities c_{ijkl} stand for the stiffnesses. On substituting Eq. (2.2) into Eq. (2.1) one obtains the fundamental equation for the components u_k of the elastic displacement $\mathbf{u}(\mathbf{r})$:

$$\sum_{j,k,l}c_{ijkl}\frac{\partial^2 u_k}{\partial x_j\partial x_l}=0 \text{ for } i=1,2,3\ . \tag{2.3}$$

To gain access to the most general situation we first consider the case of isotropic crystal symmetry. Equation (2.3) then takes the form

$$-c_{11}\nabla(\nabla\cdot\mathbf{u})+c_{44}\nabla\times(\nabla\times\mathbf{u})=0\ , \tag{2.4}$$

where we have used Voigt's notation for the elastic constants. We now partition $\mathbf{u}$ into a curl-free component and a remainder with zero divergence

$$\mathbf{u}=-\nabla\phi+\nabla\times\mathbf{A}\ . \tag{2.5}$$

To make this decomposition unique we gauge $\mathbf{A}$ by setting

$$\nabla\cdot\mathbf{A}=0\ . \tag{2.6}$$

Inserting Eq. (2.5) into Eq. (2.4) and employing Eq. (2.6) one obtains

$$-\nabla\hat{\phi}+\nabla\times\hat{\mathbf{A}}=0\ , \tag{2.7}$$

where $\hat{\phi}$ and $\hat{\mathbf{A}}$ may be interpreted as inhomogeneities of Poisson-type equations for ϕ and $\mathbf{A}$:

$$\begin{aligned} c_{11}\Delta\phi&=-\hat{\phi}\ ,\\ c_{44}\Delta\mathbf{A}&=-\hat{\mathbf{A}}\ . \end{aligned} \tag{2.8}$$

As becomes evident from forming, respectively, the divergence and the curl of Eq. (2.7), $\hat{\phi}$ and $\hat{\mathbf{A}}$ are solutions to the Laplace equation. We may hence expand the scalar elastic potential $\phi(\mathbf{r})$

$$\phi(\mathbf{r})=\sum_{l=0}^{l_{\max}}\sum_{m=-l}^{l} c_{lm}^{(1)} r^{l} Y_{lm}(\vartheta,\varphi)$$
$$+\sum_{l=0}^{l_{\max}}\sum_{m=-l}^{l} d_{lm}^{(1)} r^{l+2} Y_{lm}(\vartheta,\varphi)$$
$$+\sum_{l=0}^{l_{\max}}\sum_{m=-l}^{l} c_{lm}^{(2)} r^{-(l+1)} Y_{lm}(\vartheta,\varphi)$$
$$+\sum_{l=0}^{l_{\max}}\sum_{m=-l}^{l} d_{lm}^{(2)} r^{-(l-1)} Y_{lm}(\vartheta,\varphi) \ . \tag{2.9}$$

Here we have introduced spherical coordinates r,ϑ,φ with respect to an origin that should be preferably chosen near the center of the grain which the expansion refers to. For the space outside the grains—if this region is included in the expansion—the origin has to be chosen close to the center of gravity of the grains. The functions $Y_{lm}(\vartheta,\varphi)$ in the above expansion denote spherical harmonics. Obviously each term under the first and third sums satisfies the Laplace equation. If one expands $\hat{\phi}(\mathbf{r})$ in analogy to these sums and forms the Poisson integral, one obtains the second and fourth sums in Eq. (2.9). The vector potential $\mathbf{A}(\mathbf{r})$ may be expanded similarly, the only difference being that one has to observe Eq. (2.6). One can easily see that $r^{l}Y_{lm}(\vartheta,\varphi)$ may be reexpressed as a linear combination of products $x^{i}y^{j}z^{k}$, where $i+j+k=l$ and x,y,z denote Cartesian coordinates. If one exploits this property and inserts $\phi(\mathbf{r})$ and $\mathbf{A}(\mathbf{r})$ into Eq. (2.5), the result may be cast as

$$\mathbf{U}^{(\alpha)}(\mathbf{r})=\sum_{l,m} a_{lm}^{(\alpha)} \mathbf{u}_{lm}^{(\alpha)}(\mathbf{r}) \ , \tag{2.10}$$

where $\alpha=0$ refers to basis functions that decrease monotonically. The embedded grains are numbered $\alpha=1,2,\ldots,N$. The new expansion coefficients $a_{lm}^{(\alpha)}$ are linear combinations of the previously introduced coefficients, and the new basis functions are defined:

$$\mathbf{u}_{lm}^{(\alpha)}(\mathbf{r})=\sum_{k=0}^{l}\sum_{j=0}^{l-i} \mathbf{b}_{lmij}^{(\alpha)} x^{i}y^{j}z^{l-i-j} \ , \tag{2.11}$$

for $\alpha=1,2,\ldots,N$, and

$$\mathbf{u}_{lm}^{(0)}(\mathbf{r})=r^{-2l-3}\sum_{i=0}^{l+2}\sum_{j=0}^{l+2-i} \mathbf{b}_{lmij}^{(0)} x^{i}y^{j}z^{l+2-i-j} \ . \tag{2.12}$$

The above considerations concerning Eq. (2.10) may be generalized to find basis functions in terms of which the displacement inside the grains may be expanded in the more general case of elastic anisotropy. This can be accomplished by inserting Eq. (2.11) into Eq. (2.3). One obtains a sum of products $x^{i}y^{j}z^{k}$ with certain prefactors that are c_{ijkl}-dependent linear combinations of the coefficients $b_{lmijk}^{(\alpha)}$. In equating these linear combinations to zero one arrives at a set of $l(l+1)/2$ equations which can be solved for $b_{lmijk}^{(\alpha)}$. The number of the latter for fixed k, l, and m is $(l+2)(l+1)/2$. Since

$$(l+2)(l+1)/2-l(l-1)/2=2l+1 \ ,$$

we can construct $2l+1$ different sets of these coefficients. Each set can be labeled by the index m which runs, e.g., from $-l$ to $+l$. Substituting these coefficients into Eq. (2.11) we obtain for each grain altogether $3(l_{\max}+1)^2$ basis functions $\mathbf{u}_{lm}^{(\alpha)}(\mathbf{r})$ whose simple algebraic form alleviates considerably the calculation of expressions that involve these functions.

To render the problem physically defined, we assume that the cluster be subject to a homogeneous deformation everywhere at its surface. This amounts to assuming a homogeneous displacement $\mathbf{U}^{(0)}(\mathbf{r})$ at the surface.

At the grain boundaries, the displacement and the normal stress $\mathbf{t}_n$ must be continuous, that is

$$\mathbf{U}^{(\alpha')}|_{A_{\alpha',\alpha}}=\mathbf{U}^{(\alpha)}|_{A_{\alpha',\alpha}}$$

and (2.13)

$$\mathbf{t}_n^{(\alpha')}|_{A_{\alpha',\alpha}}=\mathbf{t}_n^{(\alpha)}|_{A_{\alpha',\alpha}} \ .$$

In practice, expansion (2.10) has to be truncated, of course, at some cutoff value of l which we have already tacitly introduced as $l_{\max}$. As a consequence of this, the respective expansions for $\mathbf{U}$ and $\mathbf{t}_n$ cannot be expected any more to satisfy exactly the boundary conditions (2.13), at least not in general. For this reason, we relax these conditions by the requirement that the associated mean-square error

$$E^2:=\sum_{\alpha',\alpha}\int_{A_{\alpha',\alpha}}\{|\mathbf{U}^{(\alpha')}(\mathbf{r})-\mathbf{U}^{(\alpha)}(\mathbf{r})|^2$$
$$+\lambda|\mathbf{t}_n^{(\alpha')}(\mathbf{r})-\mathbf{t}_n^{(\alpha)}(\mathbf{r})|^2\}d^2r \tag{2.14}$$

attain a minimum. The positive quantity λ denotes a weight which is adjusted such that the two portions of the integrand contribute with approximately the same magnitude to the mismatch. On inserting $\mathbf{U}^{(0)}(\mathbf{r})$ and Eq. (2.10) into the above expression for E^2 we obtain terms that are, respectively, linear and quadratic in the expansion coefficients $a_{lm}^{(\alpha)}$, and there is an additional constant term. Minimization of E^2 leads to a set of linear inhomogeneous equations which we cast as

$$\underline{M}\mathbf{a}=\mathbf{I} \ . \tag{2.15}$$

The inhomogeneity results from the given displacement $\mathbf{U}^{(0)}(\mathbf{r})$ at the surface. If one solves Eq. (2.15) for the coefficients $\mathbf{a}$, the displacement field $\mathbf{U}^{(\alpha)}(\mathbf{r})$ and hence $\underline{\epsilon}(\mathbf{r})$ is known within each grain. We can then form the averages of $\underline{\epsilon}(\mathbf{r})$ and $\underline{\sigma}(\mathbf{r})$ over the volume of the cluster:

$$\overline{\epsilon_{ij}}=\frac{1}{V}\int_V \epsilon_{ij}(\mathbf{r})dV \ , \tag{2.16}$$

$$\overline{\sigma_{ij}}=\frac{1}{V}\int_V \sigma_{ij}(\mathbf{r})dV \ . \tag{2.17}$$

The effective elastic moduli are defined as interconnecting $\overline{\underline{\sigma}}$ and $\overline{\underline{\epsilon}}$ through Eq. (2.10):

$$\overline{\sigma_{ij}} = \sum_{k,l} c^{\text{eff}}_{ijkl} \overline{\epsilon_{kl}} \ . \tag{2.18}$$

The fourth-rank tensor of these elastic constants consists of 21 independent components which can be determined with the aid of Eq. (2.18) if one calculates $\overline{\underline{\epsilon}}$ and $\overline{\underline{\sigma}}$ for six linearly independent homogeneous deformations at the cluster surface.

Because of practical limitations one is forced to keep the size of the cluster considerably smaller than the size of a typical macroscopic sample, and it is actually this system whose elastic properties are the subject of the calculation. If the sample would have the shape of a circular cylinder with planar top and bottom faces and if one would subject the entire surface to a homogeneous deformation, the resulting surface normal stress would be a function that varies steeply as one goes from grain to grain and its amplitude would be sizably larger than along some similarly shaped virtual face farther into the material. Hence, there is a near-surface region where the stresses behave differently from their typical spatial variation in the bulk. However, in a macroscopic sample this region is so small compared to the remaining volume that its presence does not affect the average elastic stresses. For the small samples (clusters) which our calculation refers to, this is no longer the case. In order to minimize this surface effect we use the trick of embedding the cluster in a homogeneous medium whose elastic properties agree approximately with the average properties of the cluster. As before, we subject the surface (now actually the embedding-medium–cluster-surface) to a homogeneous deformation, but because the embedding material simulates average elastic behavior, the surface effect practically disappears.

III. RESULTS AND DISCUSSION

A delicate practical problem of our approach consists in the proper choice of the cutoff value $l_{\max}$ in expansion (2.10) for the displacement. If one were forced to include a very large number of expansion terms (e.g., >50 per grain) to ensure a judicious accuracy for the envisaged effective moduli, one would quickly run into computational difficulties. For this reason it is indispensable to test the scheme with simple systems which have been investigated by other authors using different methods. A spherical grain embedded in a homogeneous medium constitutes a well-studied example of this kind.[4–8] In this case one assumes that the system is subject to an asymptotically homogeneous strain so that the calculation of the displacement field in the embedding medium is part of the problem. This means that one needs an expansion for this region as well with different (decreasing) basis functions as defined by Eq. (2.12). The strain inside the spherical grain was shown by Eshelby[5] to be constant. Outside the sphere the strain field proves to be quadrupole-type. Hence, for the displacement one has in this case a natural expansion cutoff at $l_{\max}=1$ and $l_{\max}=3$, respectively. Figure 1 shows the result of our calculation in terms of the relative changes of the specific volume

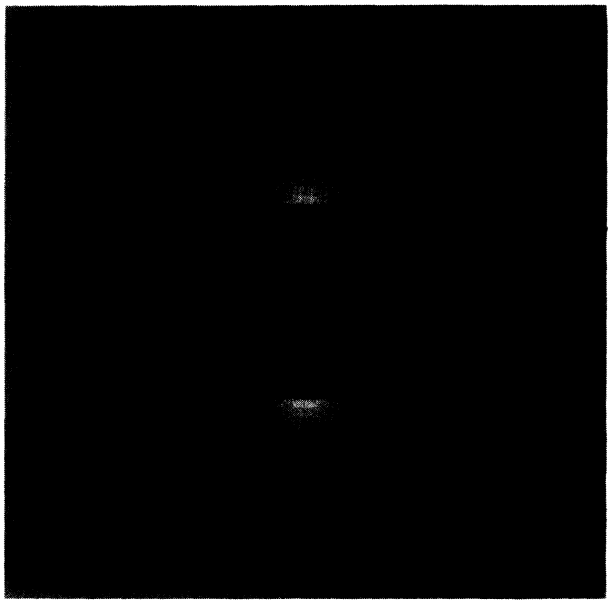

FIG. 1. Relative changes (coded in half-tone steps) of the specific volume $\delta v(\mathbf{r})/v_0$ in a system consisting of a spherical grain in an isotropic embedding matrix subject to a uniaxial strain. The cut is taken through the center of the sphere along the plane $z=0$ containing the strain axis.

$$\frac{\delta v(\mathbf{r})}{v_0} = \mathrm{Tr}[\underline{\epsilon}(\mathbf{r}) - \underline{\epsilon}_0] \tag{3.1}$$

for a uniaxial strain whose asymptotic portion is denoted by $\underline{\epsilon}_0$. We have used this model in a previous study[13] to calculate the elastic moduli of isotropic crystalline materials. If one replaces the spherical grain by a cube, one obtains a system that constitutes a considerably more demanding test case in that the truncation of our expansion (2.10) may now give rise to errors. We have used a cutoff value $l_{\max}=5$ for the expansion inside and outside the cube. As one can see from Fig. 2 the characteristic features of $\delta v(\mathbf{r})/v_0$ outside remain the same, whereas inside $\delta v(\mathbf{r})/v_0$ is now far from being constant. Though this particular system seems to be of no great relevance to the treatment of realistic polycrystals, it provides some insight into a welcome limitation of our method which is reflected in the relatively smooth spatial dependence of the stresses close to the corners of the cube where the true variation is actually strongly peaked. However, the percentage of the volume in which our expansion fails to give a sufficiently accurate description of the stresses is so small that the associated error will affect the volume average of the stresses only minutely. On the other hand, from a calculational point of view there is much reason for retaining the principal shape of such a grain with rectangular corners. The form of our basis functions, defined by Eq. (2.11), suggests a natural preference for grain shapes of this kind. Hence, if we construct apparently unrealistic clusters out of grains with rectangu-

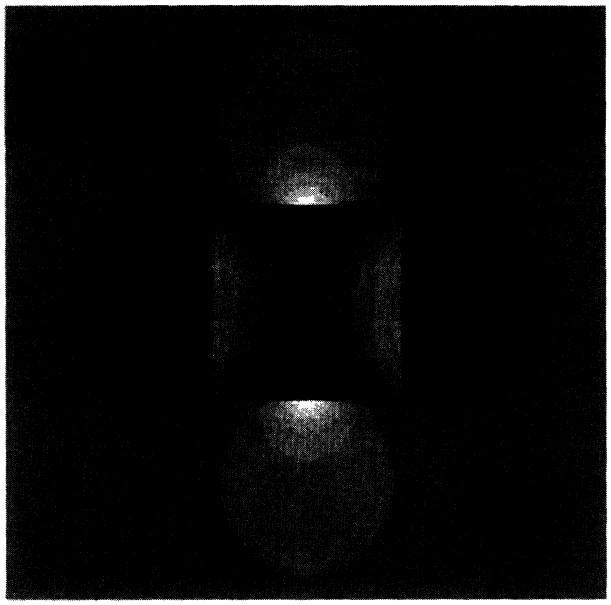

FIG. 2. The function $\delta v(\mathbf{r})/v_0$ for a cubical grain embedded in an isotropic matrix. As in Fig. 1 (with identical geometry) the system is subject to a uniaxial strain.

lar corners, we may, nevertheless, expect our calculation to yield very reasonable results because our expansions do not resolve the existence of the actually unrealistic grain corners. An example of such a cluster that consists of cubical grains is given in Fig. 3 where we show again the variation of $\delta v(\mathbf{r})/v_0$. The external primary strain is identical to the situation in Fig. 1, the only difference being that we have replaced the spherical grain with the cubical cluster. The function $\delta v(\mathbf{r})/v_0$ does obviously not provide a suitable description of the elastic deformation in such a structure if one wants to assess the quality of the convergence of our expansions, as $\delta v(\mathbf{r})/v_0$ must be for physical reasons discontinuous at the grain boundaries. On the other hand, it is just this property which brings out very clearly that the crystal axes of the grains shown in Fig. 3 are all differently oriented, actually at random in the present case. The latter becomes particularly apparent from Fig. 4 where we have plotted the displacement field $\Delta\mathbf{U}(\mathbf{r})=\mathbf{U}(\mathbf{r})-\mathbf{U}_0(\mathbf{r})$ for the same situation Fig. 3 refers to. (Here $\mathbf{U}_0$ denotes the homogeneous displacement field to which $\underline{\epsilon}_0$ is connected.) We have indicated the direction and absolute value of $\Delta\mathbf{U}(\mathbf{r})$ by arrows with varying lengths. Obviously, $\Delta\mathbf{U}(\mathbf{r})$ is everywhere continuous and smooth within the accuracy of this plotting technique. This means that the grain boundaries have become invisible, and the randomness of the orientations of the crystal axes is mirrored in the chaotic flow of $\Delta\mathbf{U}(\mathbf{r})$.

We have first applied our method to macroscopically isotropic materials by treating a cubical section out of the respective polycrystal which we subdivide into 7^3 cubes of single crystals whose crystallographic axes were randomly distributed using a random generator. The results are compiled in Tables I and II where we have also listed the lower and upper bounds according to Reuss and Voigt, respectively, and the values of the narrower bounds due to Hashin and Shtrikman. In comparing the scattering of data in the literature concerning elastic constants of single crystals and their polycrystalline counterparts, one notices a striking difference in that the results

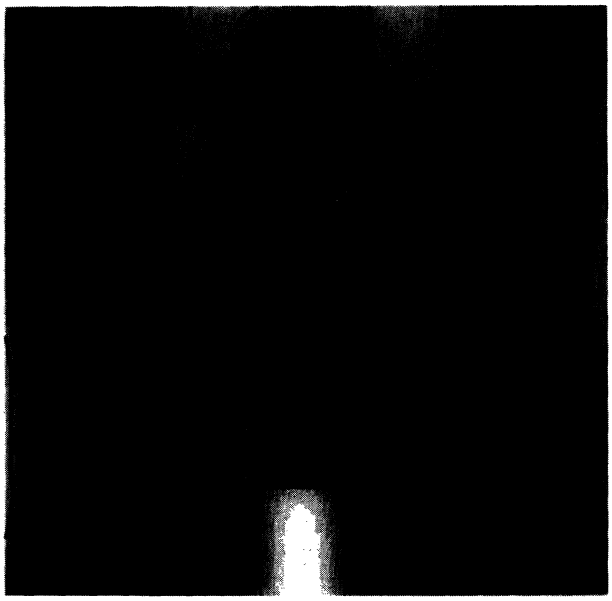

FIG. 3. The function $\delta v(\mathbf{r})/v_0$ describing the elastic deformation in a cubical cluster of cubical grains. The situation is identical to what Fig. 1 refers to except that the sphere has been replaced with a cubical cluster.

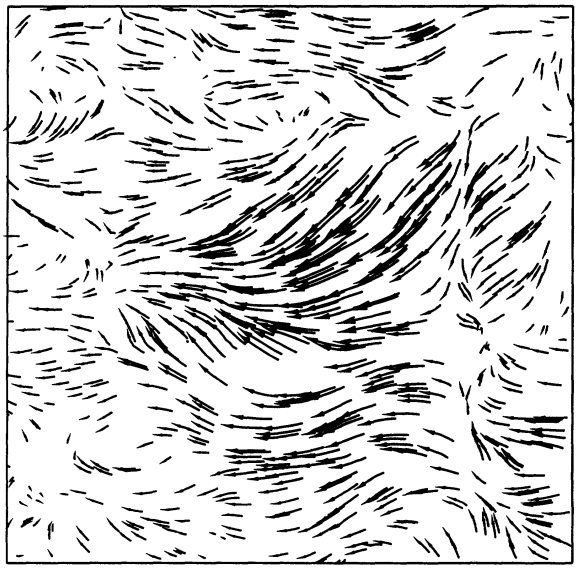

FIG. 4. The displacement $\Delta\mathbf{U}(\mathbf{r})=\mathbf{U}(\mathbf{r})-\mathbf{U}_0(\mathbf{r})$ associated with the elastically deformed cluster shown in Fig. 3. Length and direction of the arrows refer to the absolute value and the direction of $\Delta\mathbf{U}(\mathbf{r})$, respectively.

TABLE I. Theoretical and experimental results for the bulk modulus (B) of polycrystalline metals in GPa. If not stated differently, the experimental data originate, in principle, from Ref. 15 but had to be converted to the bulk modulus listed here. The data concerning the trigonal materials bismuth metal and quartz are also referred to by Kumar (Ref. 14).

	Bulk modulus B Theory					
	Reuss	HS1	Cluster	HS2	Voigt	Expt.
Cubic						
Ag[a]	102.3	102.3	102.3	102.3	102.3	96
Al[a]	77.3	77.3	77.3	77.3	77.3	70
Au[a]	170.7	170.7	170.7	170.7	170.7	164
Cu[b]	137.6	137.6	137.6	137.6	137.6	144
Fe[a]	166.7	166.7	166.7	166.7	166.7	167
K[a]	3.35	3.35	3.35	3.35	3.35	4.1
Mo[c]	263.7	263.7	263.7	263.7	263.7	301
Na[a]	6.75	6.75	6.75	6.75	6.75	7.4
Ni[a]	184.3	184.3	184.3	184.3	184.3	205
Pb[a]	43.9	43.9	43.9	43.9	43.9	34
Hexagonal						
Be[a]	11.3	111.5	111.4	111.5	111.7	114
Cd[a]	48.9	53.3	55.4	56.1	59.0	46
Co[a]	187.4	187.4	187.4	187.4	187.4	184
Mg[a]	35.2	35.2	35.2	35.2	35.2	49
Ti[b]	104.4	104.5	104.5	104.5	104.6	111
Zn[b]	62.0	66.9	69.7	70.2	73.0	69.4[h]
Zr[a]	96.5	96.6	96.6	96.6	96.7	91
Graphite[a]	35.8	42.0	58.7	204.2	286.3	
Tetragonal						
Sn[a]	57.0	57.0	57.0	57.0	57.0	56
$BaTiO_3$[d]	136.8	138.0	138.6	138.6	139.1	106[i]
$Bi_2Sr_2CaCu_2O_8$[e]	69.9	73.9	76.0	76.1	78.7	30.8[j]
La_2CuO_4[f]	112.8	112.8	112.8	112.8	112.8	122.0[k] 87[l]
$YBa_2Cu_3O_7$[g]	113.7	114.8	115.4	115.3	115.9	120[m] 68.5[n]
Trigonal						
Bi	32.5	33.5	33.9	34.0	34.7	34.1
Quartz	37.4	37.6	37.6	37.7	37.9	39.2

[a]Single-crystal data from Ref. 16.
[b]Single-crystal data from Ref. 17.
[c]Single-crystal data from Ref. 18.
[d]Single-crystal data from Ref. 19.
[e]Single-crystal data from Refs. 20 and 21.
[f]Single-crystal data from Ref. 22.
[g]Single-crystal data from Ref. 23.
[h]From Ref. 17.
[i]From Ref. 24.
[j]From Ref. 25.
[k]From Ref. 26.
[l]From Ref. 27.
[m]From Ref. 28.
[n]From Ref. 29.

for single crystals seem to be relatively uniform (i.e., rather accurate) whereas there is a large scatter in the polycrystalline data. It is obviously very difficult to manufacture ideally structured polycrystalline materials and to ensure the same degree of purity as with single crystals. We are hence led to conclude that a comparison of the calculated elastic constants with experimental data can hardly serve as a clue for the quantitative capabilities of our method. As already mentioned, one has to keep the number of grains in a cluster as small as possible for reasons of computational feasibility. It is therefore indispensable to find a criterion for the minimal number of grains required to simulate the polycrystalline material with sufficient accuracy. The so-called anisotropy has proven to be a very sensitive criterion of this kind. It is defined by

$$A_G = \frac{G_{\max}}{G_{\min}} ,$$

$$A_E = \frac{E_{\max}}{E_{\min}} ,$$

where A_G is a generalization of the Zener anisotropy which refers to cubic materials. For a truly isotropic polycrystal A_G and A_E must be equal to one. It is obvious from this property that a departure from unity immediately indicates deficiencies of the calculation. The usefulness of this criterion is demonstrated in Fig. 5 where we marked by respective symbols the calculated anisotropy A_G of Cu, Zn, and Ti clusters as a function of the number of grains. One clearly recognizes that the anisotropy drops off towards unity as the number of grains increases. Evidently, the anisotropy has already leveled off at a nearly constant value beyond ~ 200 grains so that one would not gain much improvement on pushing up the calculation up to even 1000 grains. Only if one would enlarge the number of grains by a factor of 10 one might be able to achieve a result that is still better converged. Since any practical calculation for A_G and A_E will always yield a departure from unity, it is instructive to study the dependence of this departure as a function of the anisotropy of the pertinent single crystal. Of course, one expects that cluster and single-crystal anisotropies increase in a correlated way. To show that, we have performed calculations on the same materials as in Tables I and II. The results are listed in Table III. For the sake of a better assessment of trends referred to above, we have displayed the results in Figs. 6 and 7 as a dependence of the polycrystal anisotropy vs single-crystal anisotropy. Graphite plays a rather exceptional role: its anisotropy exceeds by far the range over which typical values of the remaining materials of our list extend. For this reason graphite is not included in Figs. 6 and 7. To obtain a judicious anisotropy value for the cluster it proved to be necessary to enlarge the number of grains in this case up to 8^3.

We consider it a decisive strength of our method that it can handle strongly textured materials displaying an extreme variety of grain shapes in terms of ratios c/a, where c and a are measures of typical lengths and widths

of the grain. Though the scheme requires in its present form a columnar or disclike shape of the grains and rectangular corners, this restriction does not constitute a principal limitation and will be removed in future studies. But even with this limitation still being present, we are able to study experimentally well-known fiber textures of copper wires which Figs. 8–10 refer to. Typical drawing textures of fcc metals may approximately be analyzed in terms of a superposition of two ideal orientations, viz. [100] and [111]. The abscissa in all figures is c/a, where c is the length of the grains parallel to the axis of the wire which is taken along the z direction, and a denotes the width perpendicular to this direction. The cross section is assumed to be quadratic. We have plotted the dependence of the complete set of elastic moduli that refer to axial symmetry and Young's modulus E which relates to the direction of the wire. The three plots in each panel of Fig. 8 are marked by different symbols (squares, diamonds, and asterisks). They refer to the typical [100] and [111] orientations and to the [110] orientation which is more of academic interest. Obviously, there is no c/a dependence of Young's modulus for the [100] and [111] orientations. This is a consequence of the fact that in these high-symmetry directions of a single crystal this modulus attains its maximum and minimum values, respectively. This applies more generally to the stiffness c_{33} and c_{13} which have the z axis (i.e., the axis of the wire) as one of the reference directions in common. The shear

TABLE II. Theoretical and experimental results for the shear modulus (G) of polycrystalline metals in GPa. The experimental data are taken from Ref. 15. It should be noted that we have listed the arithmetic means of the values given there.

	Shear modulus G Theory					
	Reuss	HS1	Cluster	HS2	Voigt	Expt.
Cubic						
Ag	25.6	28.9	29.5	30.6	33.4	30.1
Al	25.9	26.1	26.1	26.1	26.2	26.9
Au	23.9	27.1	28.2	28.8	31.2	26.5
Cu	40.1	46.1	47.2	49.5	54.7	48.3[a]
Fe	73.8	80.4	80.4	83.2	89.2	83.4
K	0.531	0.730	1.008	1.020	1.242	1.32
Mo	122.7	124.4	124.7	124.8	125.8	125
Na	1.29	1.74	2.10	2.34	2.83	2.99
Ni	74.5	82.0	82.0	85.3	92.0	80.0
Pb	6.73	8.13	8.97	9.19	10.36	5.67
Hexagonal						
Be	150.3	151.0	150.8	151.2	151.8	141
Cd	21.6	23.0	23.5	24.2	25.8	25.0
Co	75.3	76.6	76.3	77.1	78.3	78.9
Mg	17.2	17.3	17.3	17.3	17.4	17.5
Ti	42.8	43.7	43.7	44.1	44.8	44.2[a]
Zn	36.4	39.8	41.6	42.6	45.6	41.8[a]
Zr	36.1	36.4	36.4	36.5	36.8	25.3
Graphite	9.21	14.9	27.7	148.9	219.4	
Tetragonal						
Sn	15.6	17.7	18.9	19.0	20.1	20.5
$BaTiO_3$	52.0	55.9	58.0	59.4	64.4	44[b]
$Bi_2Sr_3CaCu_2O_8$	20.8	22.2	23.0	23.4	25.4	29.5[c]
La_2CuO_4	61.3	63.3	64.0	64.1	66.1	62.9[d]
						63[e]
$YBa_2Cu_3O_7$	54.5	59.0	61.7	62.2	66.7	58.5[f]
						57.4[g]
Trigonal						
Bi	10.8	12.1	12.4	13.0	14.5	13.10
Quartz	41.0	43.5	43.4	44.7	47.8	43.62

[a]From Ref. 17.
[b]From Ref. 24.
[c]From Ref. 25.
[d]From Ref. 26.
[e]From Ref. 27.
[f]From Ref. 28.
[g]From Ref. 29.

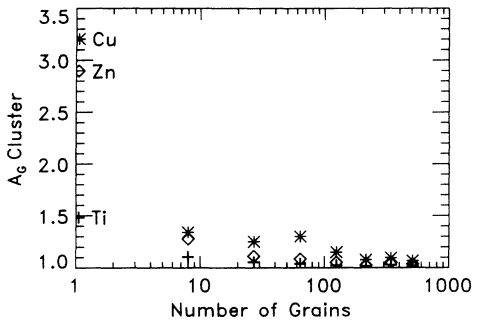

FIG. 5. Dependence of the cluster anisotropy A_G on the number of grains used in the calculation. The symbols refer to the metals Cu, Zn, Ti as indicated on the left-hand side of the diagram.

modulus G attains its maximum in the [100] direction of the single crystal. Thus, c_{44} should not display any c/a dependence for the [100] orientation.

To get an impression of the changes that take place when the two fibers occur simultaneously with a certain ratio we have in Fig. 9 plotted the resulting moduli in

TABLE III. Comparison of the cluster anisotropy to the pertinent single-crystal anisotropy.

	Single crystal		Cluster	
	A_G	A_E	A_G	A_E
Cubic				
Ag	2.923	2.675	1.0873	1.0871
Al	1.230	1.205	1.0156	1.0165
Au	2.917	2.771	1.0844	1.0884
Cu	3.205	2.864	1.0684	1.0741
Fe	2.463	2.186	1.0732	1.0692
K	7.451	6.425	1.1504	1.1484
Mo	1.385	1.324	1.0248	1.0251
Na	6.825	5.805	1.1639	1.1558
Ni	2.596	2.307	1.0781	1.0745
Pb	4.000	3.697	1.1087	1.1112
Hexagonal				
Be	1.216	1.203	1.0091	1.0259
Cd	2.349	2.768	1.0433	1.1578
Co	1.428	1.504	1.0298	1.0363
Mg	1.180	1.184	1.0136	1.0141
Ti	1.483	1.433	1.0206	1.0301
Zn	2.898	3.125	1.0357	1.1135
Zr	1.294	1.370	1.0215	1.0278
Graphite	110.00	72.07	1.3282	1.9235
Tetragonal				
Sn	3.552	2.863	1.0826	1.0900
$BaTiO_3$	3.805	2.504	1.0661	1.1068
$Bi_2Sr_2CaCu_2O_8$	3.190	2.533	1.0758	1.1433
La_2CuO_4	2.386	1.725	1.0491	1.0342
$YBa_2Cu_3O_7$	2.760	2.437	1.0475	1.1051
Trigonal				
Bi	3.347	2.840	1.0484	1.0977
Quartz	2.405	1.881	1.0283	1.0440

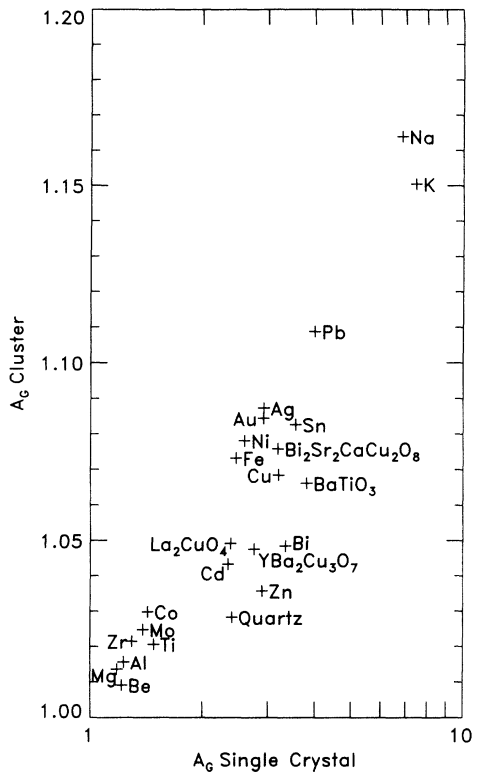

FIG. 6. Anisotropy A_G of clusters vs anisotropy of the associated single crystal. Note the logarithmic scale for the abscissa axis.

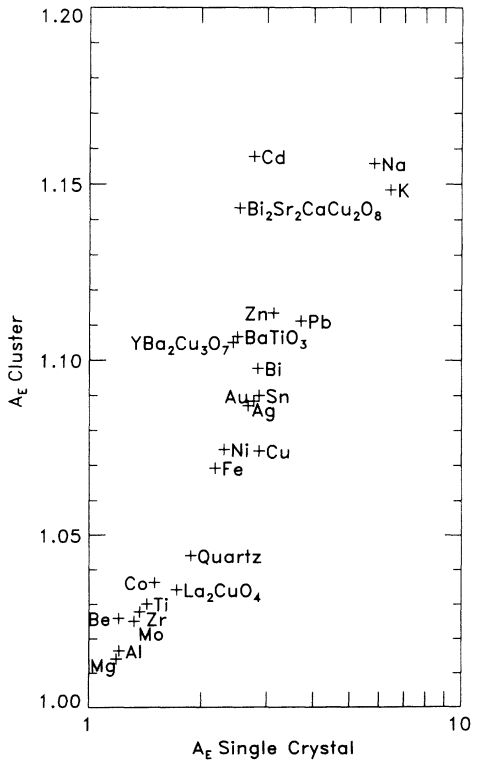

FIG. 7. Anisotropy A_E of clusters vs anisotropy of the associated single crystal.

complete analogy to Fig. 8 with the percentage of the [100] orientation as a parameter. All the data obtained lie evidently within the limits defined by the ideal orientations. In reality one is not dealing with ideal orientations which brings up the question to what extent the above results are affected by a realistic angular spread of the crystallographic axes of the individual grains. We have studied this effect by assuming a Gaussian ODF, which we write down as a probability distribution $f(\cos\vartheta)$ in the original coordinate system of the individual crystallite which the notation [111], for example, refers to. The z axis of this coordinate system makes an angle ϑ_0 with the axis of the wire. Hence, the pertinent Gaussian has the form

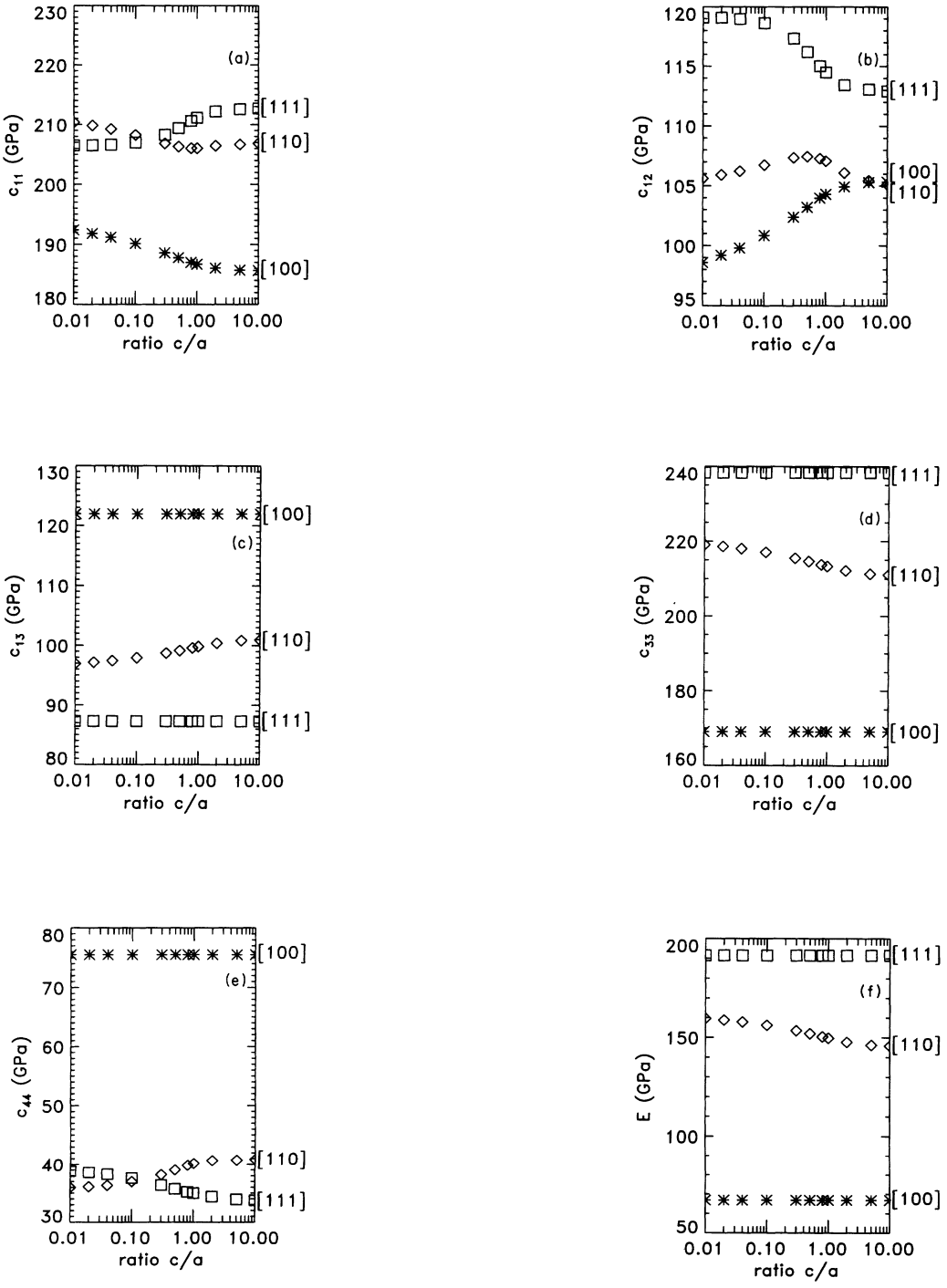

FIG. 8. Fiber textures in copper metal: elastic moduli for the ideal orientations [100], [110], and [111] as a function of the grain shape defined by the ratio c/a.

$$f(\xi)=\frac{1}{\sqrt{\pi}b/2}\exp\left[-\left[\frac{\xi-\xi_0}{b/2}\right]^2\right], \tag{3.2}$$

where b denotes the width of the distribution and $\xi=\cos\vartheta$ guarantees that the size of the orientation element in the orientation space is independent of ϑ. The results are shown in Fig. 10. For the [100] fiber texture we have assumed two spreads of the orientation, viz. $b=0.20$ and 0.06. For this particular case we have $\vartheta_0=0°$ so that we may convert these widths in terms of angular spreads of 31° and 14°, respectively. Unfortunately, this is not possible for the [111] fiber texture

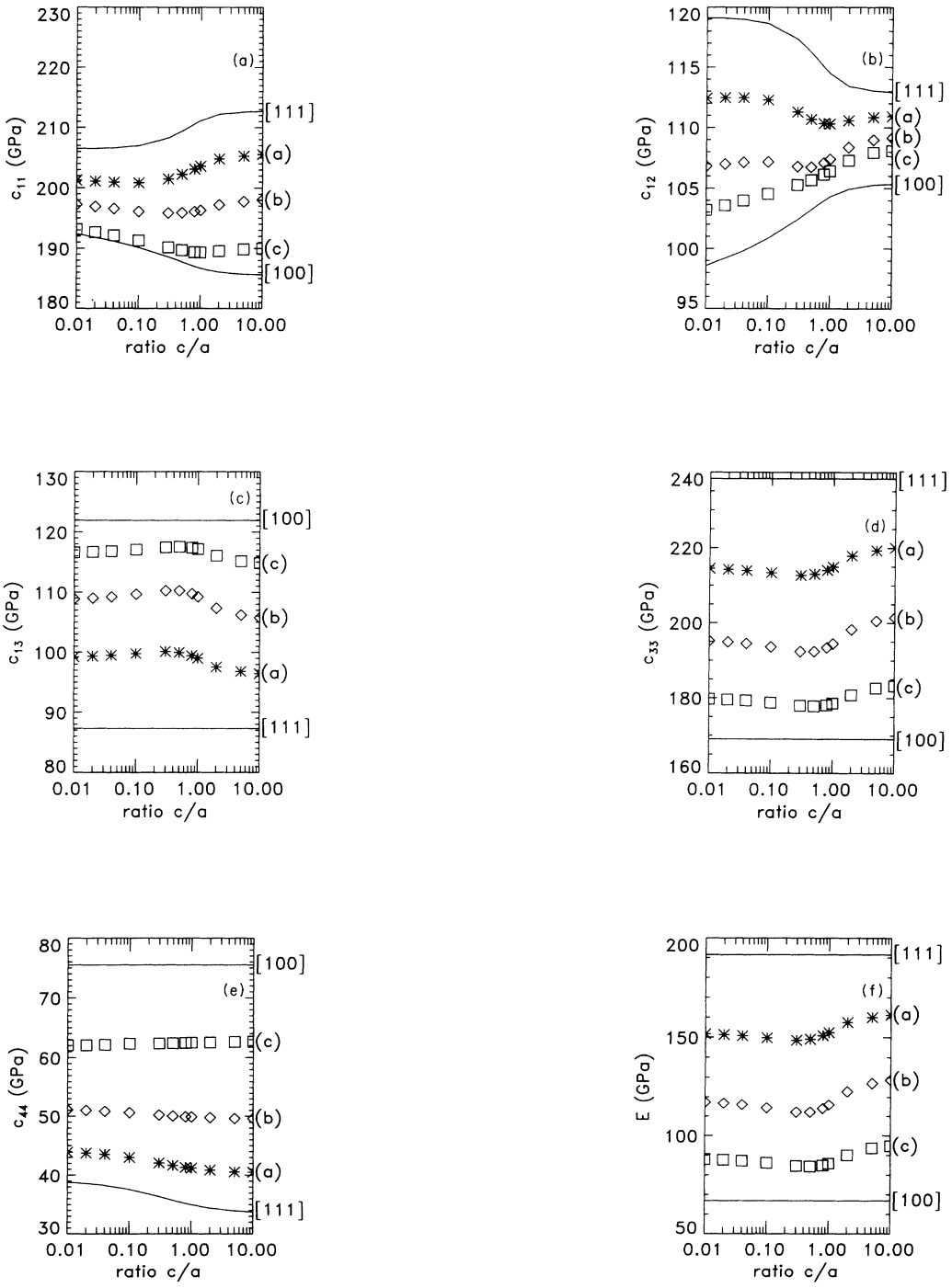

FIG. 9. c/a dependence of the elastic moduli as in Fig. 8 for a composite fiber texture of copper metal. The assumed percentages of the orientations are indicated as a parameter: (a) 23,2% [100]/76,8% [111]; (b) 45,6% [100]/ 54,4% [111]; (c) 68,8% [100]/31,2% [111]. The upper and lower solid curves refer to the pertinent ideal orientation.

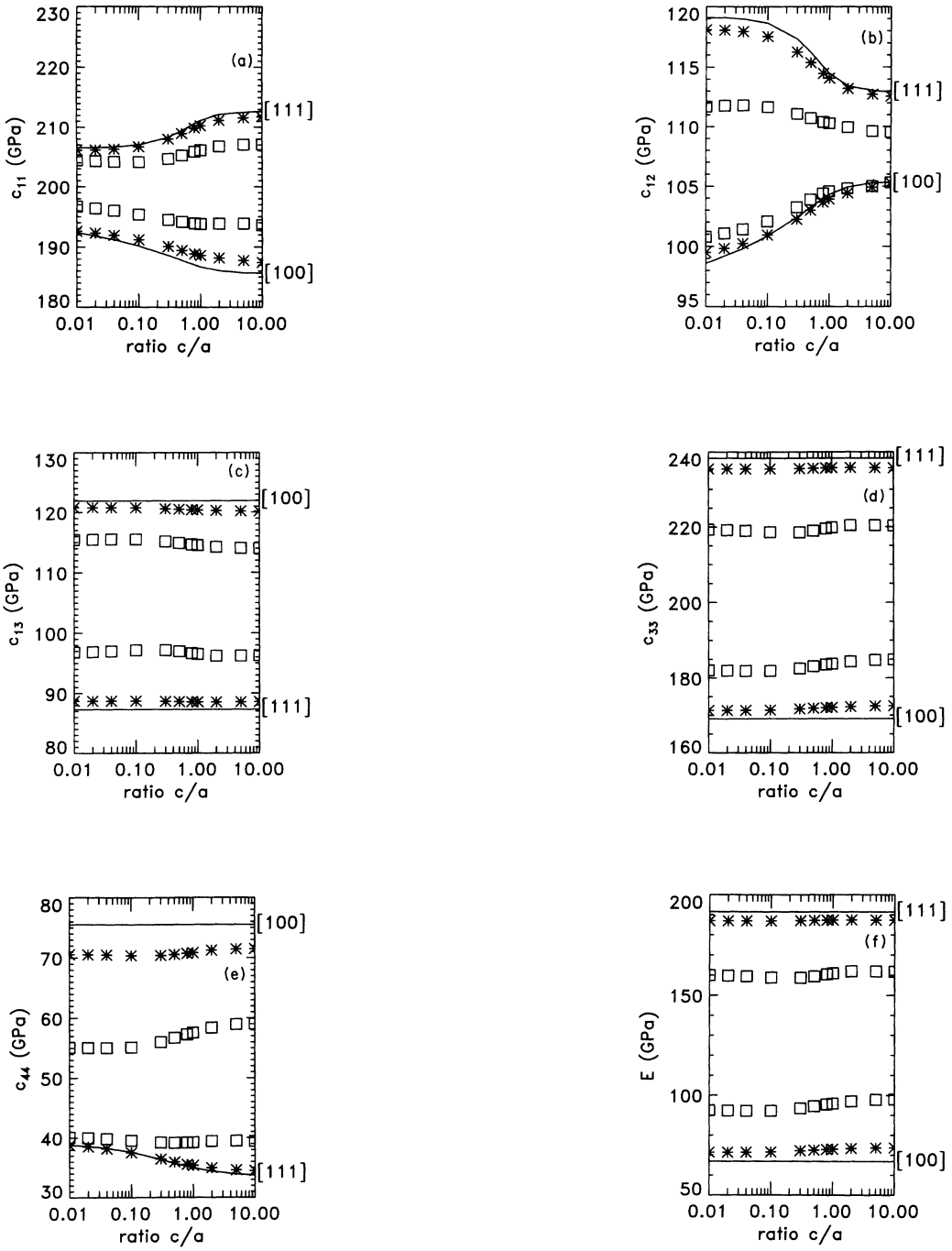

FIG. 10. c/a dependence of the elastic moduli as in Fig. 8 for fiber textures exhibiting a finite spread around the ideal orientation [100] and [111]. The latter refer to the solid curves. Results marked by asterisks and squares relate to the smaller and larger spreads, respectively.

since ϑ_0 is sizably different from zero. But it is easy to see that comparable spreads of the orientation corresponds in this case formally to larger widths which we have assumed to be $b=1.41$ and 0.28, respectively. In assessing the results one should bear in mind that an angular spread of 31° is relatively unrealistic. Typical wire samples exhibit spreads that are definitely smaller. Further work will be directed to the study of rolling textures.

ACKNOWLEDGMENTS

We wish to thank Professor H. J. Bunge (TU Clausthal) for many valuable discussions and suggestions. We are also indebted to Professor E Kröner (TU Stuttgart) for helpful comments. The present work was financially supported by the Deutsche Forschungsgemeinschaft which is gratefully acknowledged.

[1]A. Reuss, Z. Angew. Math. Mech. **9**, 49 (1929).
[2]W. Voigt, *Lehrbuch der Kristallphysik* (Teubner, Berlin, 1910).
[3]R. Hill, Proc. Phys. Soc. London, Sect. A **65**, 351 (1952).
[4]A. V. Hershey and V. Dahlgren, J. Appl. Mech. **21**, 236 (1954).
[5]J. D. Eshelby, Proc. R. Soc. London, Ser. A **241**, 376 (1957).
[6]E. Kröner, Z. Phys. **151**, 504 (1958).
[7]G. Kneer, Doctoral thesis, Technische Universität, Clausthal, 1964.
[8]G. Kneer, Phys. Status Solidi **9**, 825 (1965).
[9]E. Kröner, J. Mech. Phys. Solids **25**, 137 (1977).
[10]R. Zeller and P. H. Dederichs, Phys. Status Solidi B **55**, 831 (1973).
[11]Z. Hasin and S. Shtrikman, J. Mech. Phys. Solids **10**, 335 (1962).
[12]Z. Hashin and S. Shtrikman, J. Mech. Phys. Solids **10**, 343 (1962).
[13]H. Kiewel and L. Fritsche, Mater. Sci. Forum **157-162**, 1609 (1994).
[14]S. Kumar, Ph.D. thesis, Pennsylvania State University, 1992.
[15]*Mehanisch-Thermische Zustandsgrössen,* Landolt-Börnstein, Group 2, Vol. 1 (Springer, Heidelberg, 1971).
[16]*Elastic, Piezoelectric, and Related Constants,* Landolt-Börnstein, New Series, Group 3, Vol. 11 (Springer, Heidelberg, 1979).
[17]G. Bradfield, see Ref. 8.
[18]*Elastic, Piezoelectric, and Related Constants,* Landolt-Börnstein, New Series, Group 3, Vol. 11 Suppl. (Springer, Heidelberg, 1984).
[19]Z. Li, S. K. Chan, M. H. Grimsditch, and E. S. Zouboulis, J. Appl. Phys. **70**, 7327 (1991).
[20]M. Boekholt, J. V. Harzer, B. Hillebrands, and G Güntherodt, Physica C **179**, 101 (1991).
[21]W. Jin, W. Yening, G. Pingsheng, S. Huimin, Y. Yifeng, and Z. Zhongxian, Phys. Rev. B **47**, 2806 (1993).
[22]A. Migliori, W. M. Visscher, S. E. Brown, Z. Fisk, S. W. Cheong, B. Alten, E. T. Ahrens, K. A. Kubat-Martin, J. D. Maynard, Y. Huang, D. R. Kirk, K. A. Gillis, H. K. Kim, and M. H. W. Chan, Phys. Rev. B **41**, 2098 (1990).
[23]H. Ledbetter and L. Ming, J. Mater. Res. **6**, 2253 (1991).
[24]D. Berlincourt and H. Jaffe, Phys Rev. **111**, 143 (1958).
[25]H. Ledbetter and S. Kim, Physica C **185-189**, 935 (1991).
[26]H. Ledbetter, S. A. Kim, C. E. Violet, and J. D. Thompson, Physica C **162-164**, 460 (1989).
[27]C. Fanggao, M. Cankurtaran, G. A. Saunders, A. Al-Kheffaji, D. P. Almond, P. J. Ford, and D. A. Ladds, Phys. Rev. B **43**, 5526 (1991).
[28]B. Bridge, J. Mater. Sci. Lett. **8**, 695 (1989).
[29]M. Cankurtaran and G. A. Saunders, Phys. Rev. B **39**, 2872 (1989).

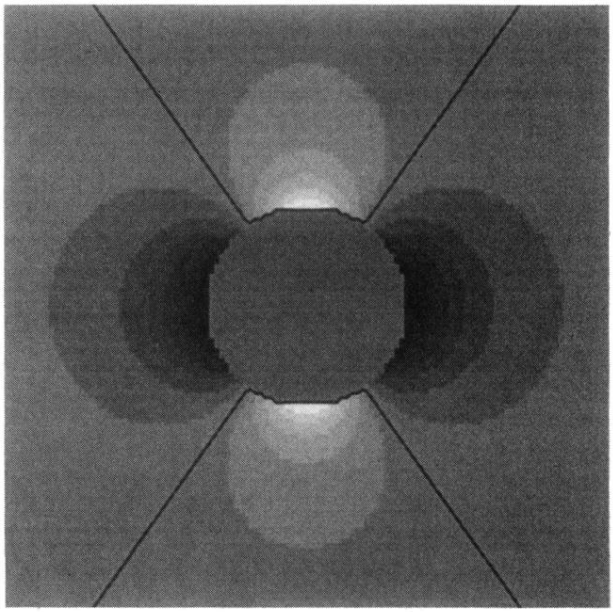

FIG. 1. Relative changes (coded in half-tone steps) of the specific volume $\delta v(\mathbf{r})/v_0$ in a system consisting of a spherical grain in an isotropic embedding matrix subject to a uniaxial strain. The cut is taken through the center of the sphere along the plane $z=0$ containing the strain axis.

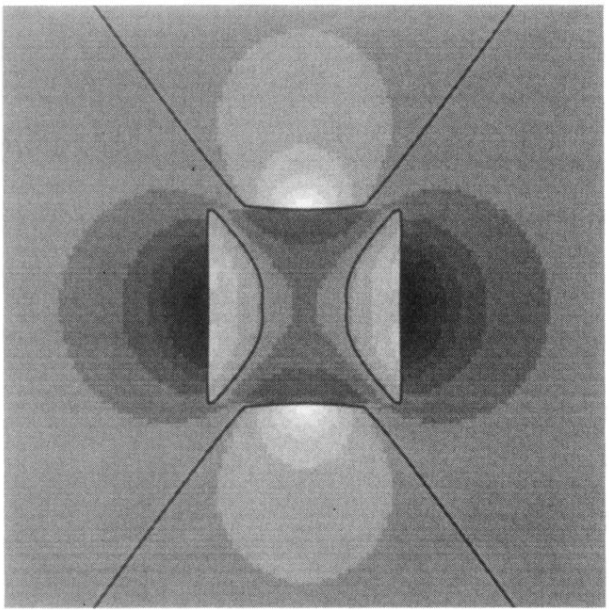

FIG. 2. The function $\delta v(\mathbf{r})/v_0$ for a cubical grain embedded in an isotropic matrix. As in Fig. 1 (with identical geometry) the system is subject to a uniaxial strain.

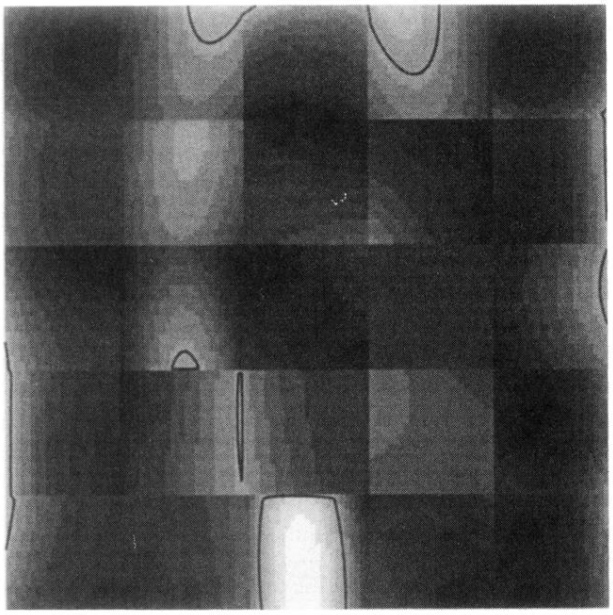

FIG. 3. The function $\delta v(\mathbf{r})/v_0$ describing the elastic deformation in a cubical cluster of cubical grains. The situation is identical to what Fig. 1 refers to except that the sphere has been replaced with a cubical cluster.